Electronic Supplementary Material (ESI) for Journal of Materials Chemistry C.

Anti-Interference Monitoring of Sweat pH：a New Sensing Mechanism Based on p-n Transition Potential of Flexible Bi_2O_3 Photoelectrode

Boheng Dong, Xinya Zhang, Lingfeng Cao, Xiang Jiang and Fuxian Wang**

Material and Methods

Materials and reagents

Metallic bismuth (Bi, 99.995 %) and indium tin oxide (ITO, In_2O_3: SnO_2=9:1) cylindrical sheet targets were obtained from ZhongNuo Advanced Material Technology Co., Ltd (China). The natural mica film (thickness 20 μm), polyethylene glycol terephthalate film (PET, thickness 50 μm), Ag/AgCl film (thickness 50 μm) and graphite paper (thickness 50 μm) were brought from taobao.com. Polydimethylsiloxane (PDMS, sylgard 184) were obtained from Dow Chemical (China) Co., Ltd. Sodium chloride (99.5 %), potassium chloride (99.5 %), acetone (99.5 %), isopropanol (99.7 %), ethanol (99.7 %), acetic acid (99.5 %) and sodium hydroxide (96%) were brought from Guangzhou Chemical Reagent Factory. Ammonium chloride (99.5 %) was obtained from Aladdin Reagent Co., Ltd (Shanghai, China). Urea (99%) and racemic lactic acid (90 %) were brought from Shanghai Mclean Biochemical Science and Technology Co. Ltd (China). Polyvinyl acetate (PVAc, 10 W molecular weight) was purchased from Wacker Chemicals (China) Co., Ltd. Graphite conductive paste is produced by Suzhou Ancnrd Electronic New Material Co., Ltd (China).

Bi_2O_3 working electrode preparation and physicochemical characterization

Bi_2O_3 working electrode (WE) was prepared using the direct-current magnetron method. The natural mica substrate was ultrasonically cleaned in acetone, isopropanol, and ethanol for 10 min respectively and dried in a stream of nitrogen. Before preparing Bi_2O_3 film, ITO film was deposited on the natural mica substrate using the direct-current magnetron method. During ITO film deposition, the sputtering power of ITO target was 100 W. Mica substrate was heated to 200 °C and kept rotating

at 20 r min^{-1}. The flow rate of argon was 30 sccm. The pressure in the vacuum chamber was maintained at 1.0 Pa and the deposition time was 2400 s. When preparing Bi_2O_3, ITO/mica as the substrate was heated to 100 °C and Bi target with 40 W power was sputtered for 240 s. The other conditions are the same as the conditions for preparing ITO. Finally, Bi_2O_3/ITO/mica was calcinated in air at 350 °C for 1 h.

Scanning electron microscope (SEM, SU8220, HITACHI) was used to obtain the morphology of the films at an acceleration voltage of 5 kV. Work function and Fermi level was obtain using the ultraviolet photoelectron spectroscopy (UPS, ESCALAB Xi+, Thermo Scientific) with He I (hv = 21.2 eV) radiation. The crystal structures of the films were investigated by X-ray diffraction (XRD, D8 Advance, Bruker) using Cu Kα radiation (λ = 0.154 nm) with a scanning speed of 5 ° min^{-1}. HITACHI U-4100 spectrophotometer was used to investigate optical performance of the film. Absorption coefficient α of the film was calculated as follows:

$$\alpha = ln\left(\frac{1}{T}\right)/d$$

where T is transmittance of the film and d is the effective thickness of the film. The band gap E_g of Bi_2O_3 was obtained by the following formula:

$$(\alpha \mathrm{hv})^{1/n} = \mathrm{A}(\mathrm{hv} - E_g)$$

where hv is photon energy and A is a constant. For direct band gap semiconductor n = 0.5 and for direct band gap semiconductor n = 2.

The samples were sterilized at high temperature (121 °C, 20 min) before the in vitro cytotoxicity test. 18 cm^2 sample was soaked in 3 mL of minimum essential medium (MEM) containing 10 % fetal bovine serum for 72 h at 37 °C to obtain a 100 % extract solution. The L-929 cells were cultured in MEM containing 10 % fetal bovine serum and antibiotics (penicillin 100 U mL^{-1}, streptomycin 100 μg mL^{-1}). The cells were made into cell suspension with trypsin. After centrifugation (200 g, 3 min), the cells were re-dispersed in fresh medium, and the cell density was adjusted to 1×10^5 cells ml^{-1}. The above cell suspension was inoculated into a 96-well culture plate (100 μL) and placed in

incubator for 24 hours (5 % CO_2, 37 °C, humidity > 90 %). After the cells grew into a monolayer, the original medium was aspirated, and then extract solutions (100 μL, 100 %, 75 %, 50 %, 25 %) were added. Each group contains 6 parallel samples. After culturing for 24 h (5 % CO_2, 37 °C), the cell morphology was observed under a microscope and the cell viability was tested. MTT (3-(4,5-dimethylthiazol-2-yl)-2,5-diphenyltetrazolium bromide) colorimetric assay was used to detect cell viability. Firstly, MTT (1 mg mL^{-1}, 50 μL) was added to each well and then the culture plates were placed in the incubator (5 % CO_2, 37 °C). After culturing for 2h, the supernatant was removed and then 100 μl of isopropanol was added to each well to dissolve the crystals. Finally, optical density (OD) was recorded at 570 nm. Cell viability was calculated as follows:

$$Cell\ viability\ (\%) = 100 \times \frac{average\ OD\ of\ experimental\ group\ samples}{average\ OD\ of\ blank\ control\ group\ samples}$$

Flexible PEC biosensor assembly

The Ag/AgCl reference electrode (RE) with KCl-containing PVAc solid-state electrolyte and PDMS junction membrane was prepared according to the method reported in the literature.[1] Specifically, KCl fine powder (5 g), PVAc (2.5 g) and acetone (15 mL) were mixed to prepare the KCl/PVAc electrolyte. KCl/PVAc (20 μL) was drip-coated on the Ag/AgCl film and dried at 80 °C for 10 minutes. Then PDMS (20 μL) was drip-coated on the KCl/PVAc/Ag/AgCl and cured at 80 °C for 1 hour.

Firstly, the WE, counter electrode (CE, graphite paper), and RE were pasted on PET using PDMS. Secondly, one end of the wire is fixed on the electrode of flexible PEC biosensor with graphite conductive paste, and the other end is connected to the miniature electronic component. Then, PDMS protective layer was coated on the electrode surface of flexible PEC biosensor and cured at 80 °C for 1 hour. Finally, the LED lamp was fixed on the back of the WE with PDMS.

Photoelectrochemical Measurements

For photoelectrodes on hard substrates, photoelectrochemical was measured in artificial sweat under illumination (415 nm, 35 mW cm^{-2}) using an CHI70E electrochemical workstation (Shanghai

Chenhua Instrument Co., Ltd., China) in a three-electrode configuration with the PEC pH biosensor as WE, a glass Ag/AgCl RE and a platinum sheet CE. For photoelectrodes on flexible substrates, artificial sweat (50 μL) was dropped on the surface of the pH biosensor to cover WE, RE and CE. The miniature intelligent electronic device was used for pH sensing. Photocurrent and dark current were obtained by scanning cyclic voltammetry in light and dark, respectively. The stability test of the electrode is to continuously scan cyclic voltammetry under light, and record the value of V_{p-n} after 3 minutes. The open circuit potential (V_{OCP}) of photoelectrodes was monitored in open circuit configuration under illumination.

The artificial sweat was prepared according to the method proposed by ISO 3160-2. Artificial sweat contains NaCl (20 g L^{-1}), NH_4Cl (17.5 g L^{-1}), urea (5 g L^{-1}), CH_3COOH (2.5 g L^{-1}) and $CH_3CH(OH)COOH$ (15 g L^{-1}). NaOH (80 g L^{-1}) was used to adjust the pH to 4 ~ 8.

Sweat pH monitoring during practical exercise

The pH monitor was worn on the subject's wrist and monitored for changes in sweat pH during running. In the meantime, sweat pH on the wrist was measured every 4 minutes by standard pH indicator paper as a reference. Informed written consent has been obtained from the participant prior to testing. All experiments were performed in compliance with the policy of the Human Research Ethics Committee of Guangdong Academy of Sciences (China National Analytical Center,Guangzhou).

Signal to noise ratio calculation

First, the open source software WebPlotDigitizer (https://automeris.io/WebPlotDigitizer/) was used to extract data of detection results from the literatures, and the time spacing between two adjacent data points was adjusted to 24 s (a data point was collected every 24 s, in this work) by the difference method. Then, the data was processed by fast Fourier transform (FFT) to obtain the frequency spectrum. In the frequency spectrum, the data with frequencies greater and less than 0.0125 Hz were processed by inverse fast Fourier transform (IFFT) to obtain noise and signal, respectively. SNR was calculated as follows:[2]

$$SNR = \frac{P_s}{P_n}$$

where P_s and P_n are the power of signal and noise, respectively. They were calculated as follows:

$$P_s = \frac{1}{N}\sum_{n=1}^{N} |signal|^2$$

$$P_n = \frac{1}{N}\sum_{n=1}^{N} |noise|^2$$

Supplementary Figures

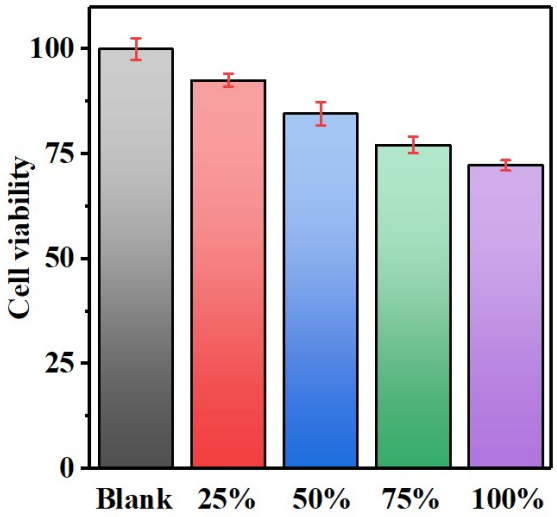

Fig. S1. Cell viability after 24 hours of culture in different concentrations of Bi_2O_3 WE extract solution.

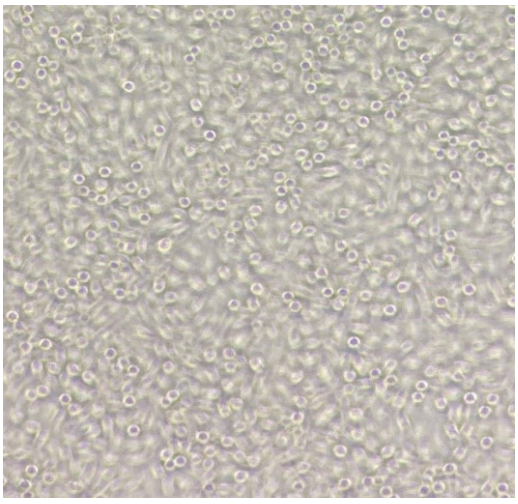

Fig. S2. Microscopic image of cells cultured in 100 % extract solution for 24 hours.

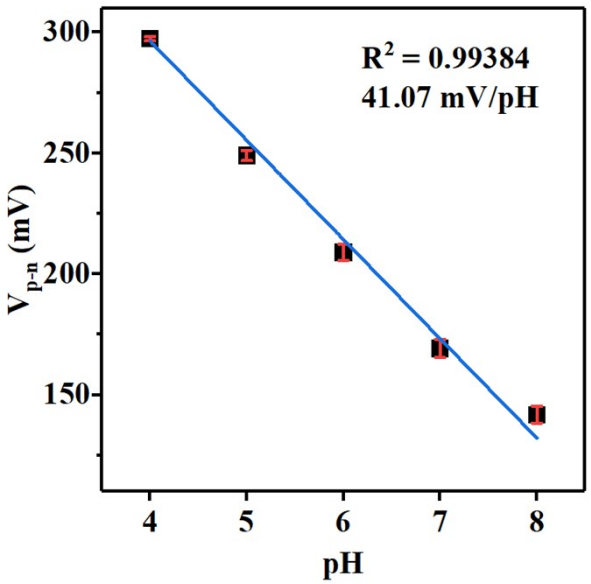

Fig. S3. Standard curve obtained with two electrode configuration.

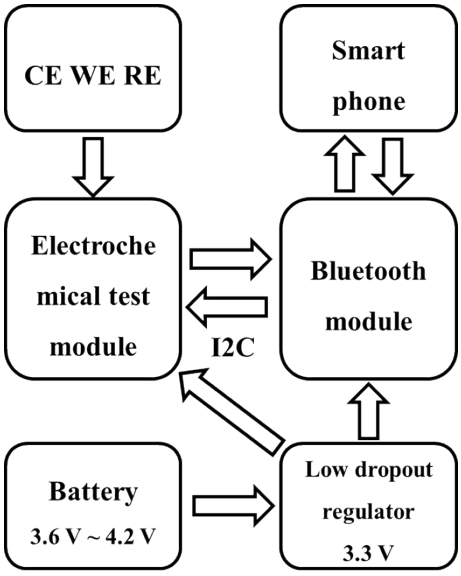

Fig. S4. overview of the flexible wearable photoelectrochemical sweat pH monitor.

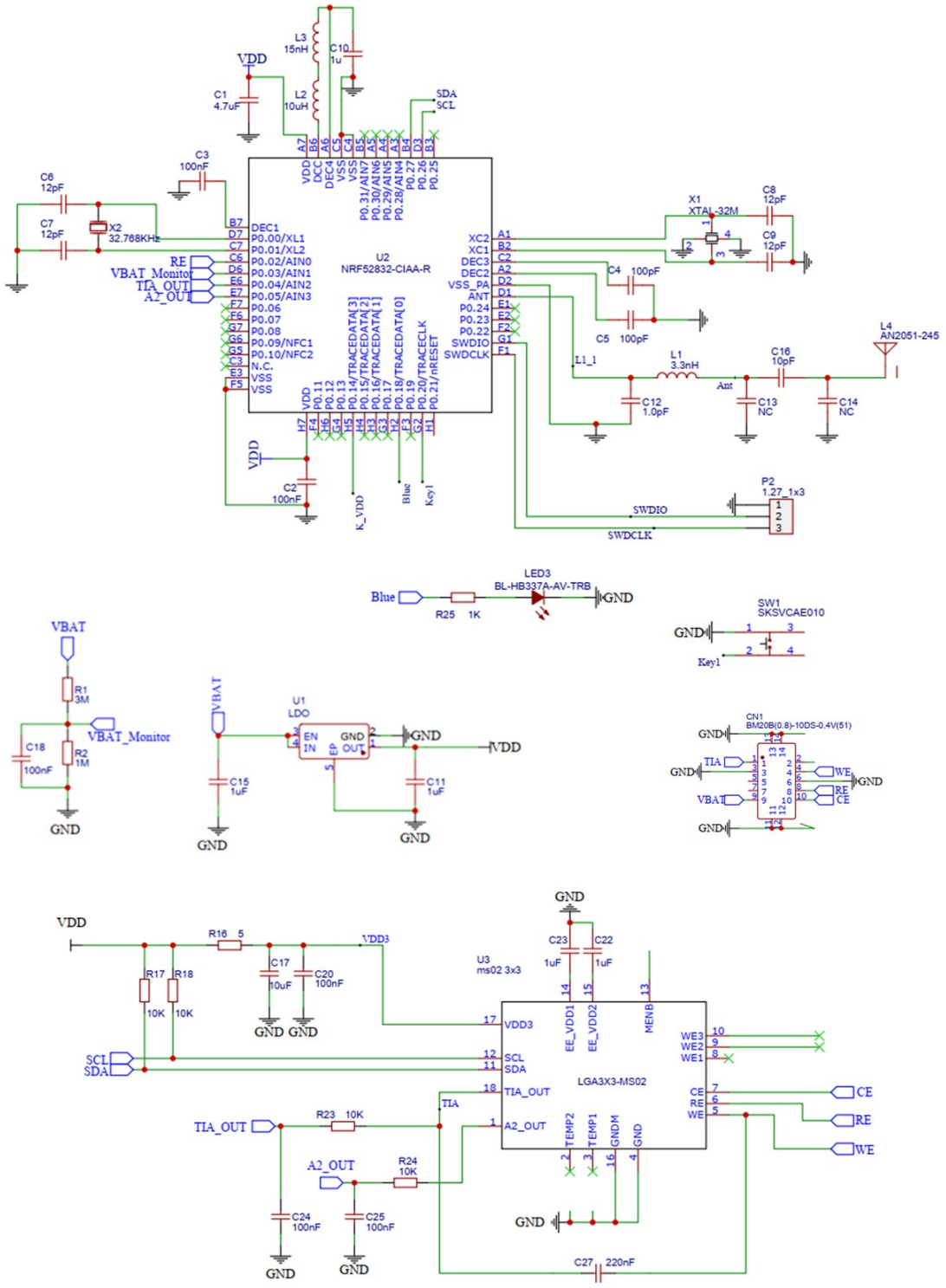

Fig. S5. Detailed schematics of the design of miniature electronic component.

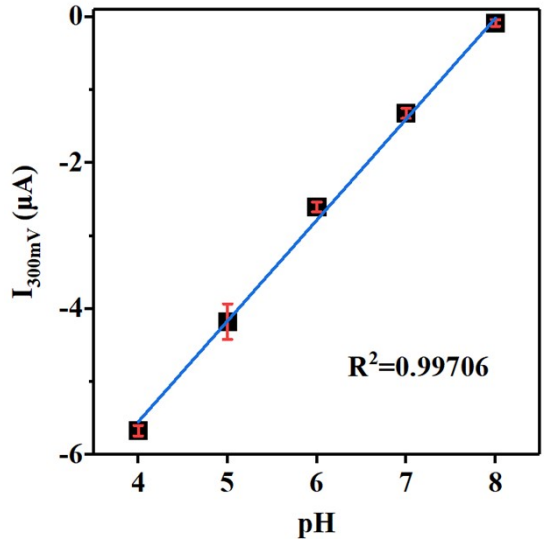

Fig. S6. Standard curve obtained by sensing signal I_{300mV}.

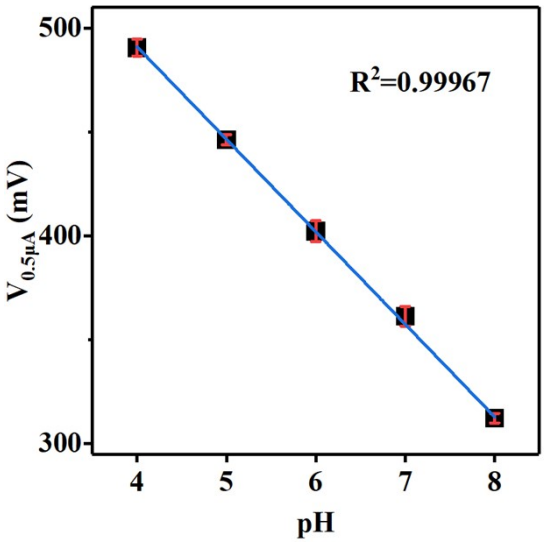

Fig. S7. Standard curve obtained by sensing signal $V_{0.5\mu A}$.

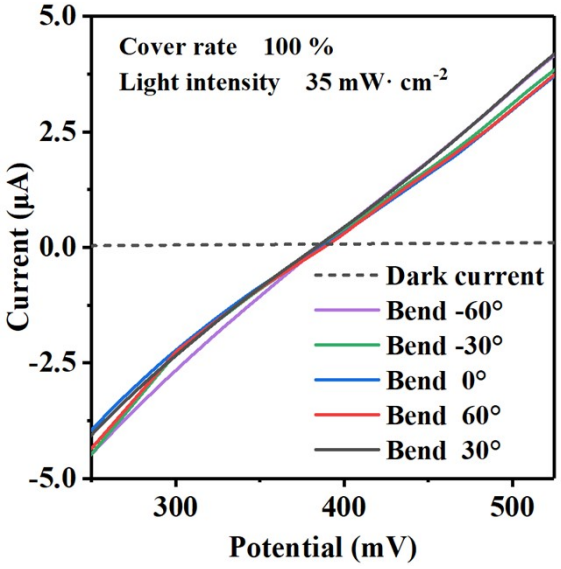

Fig. S8. CV scans for pH monitor in artificial sweat with pH 6 under conditions of the sensor bending.

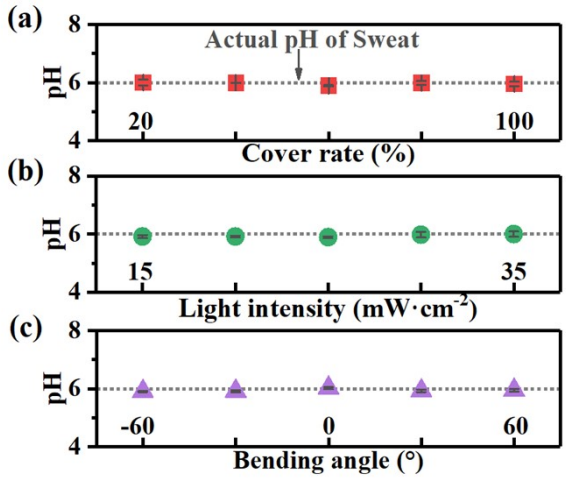

Fig. S9. pH measured by pH monitor using $V_{p\text{-}n}$ as the sensing signal under conditions of the change in (a) the sweat coverage on photoelectrode, (b) the variation in light intensity and (c) the sensor bending.

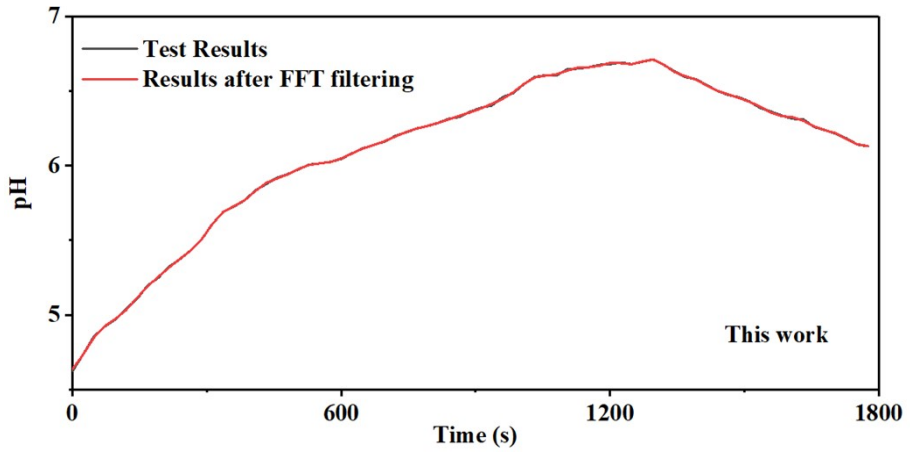

Fig. S10. Test results obtained in this work during practical exercise and results after FFT filtering.

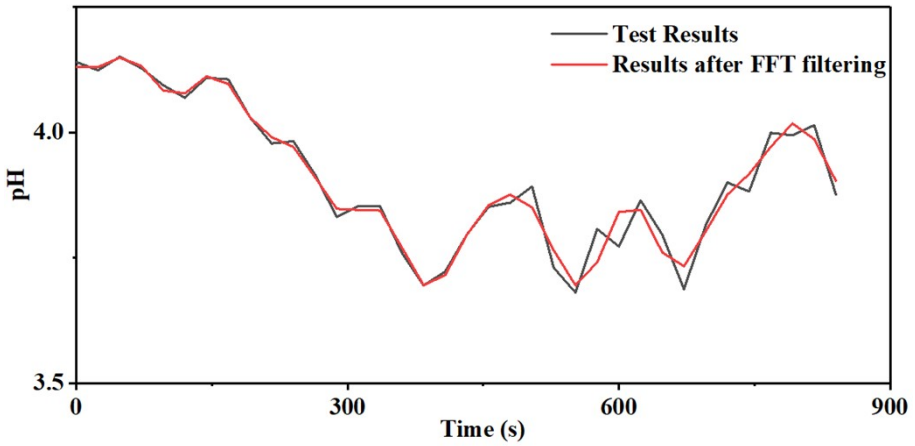

Fig. S11. Test results obtained in reference (T. Terse-Thakoor *et al.*, *npj Flexible Electron*. 2020, 4, 18.) during practical exercise and results after FFT filtering.

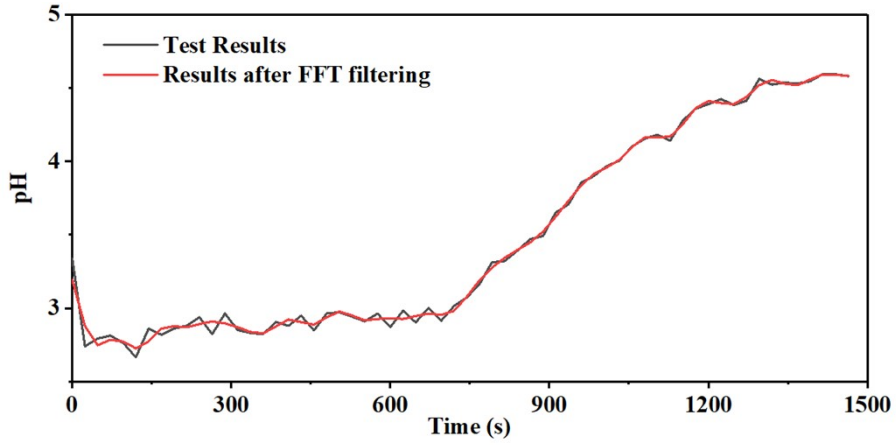

Fig. S12. Test results obtained in reference (M. Caldara *et al.*, in *2013 IEEE International Conference on Body Sensor Networks*, 2013, pp. 1-6.) during practical exercise and results after FFT filtering.

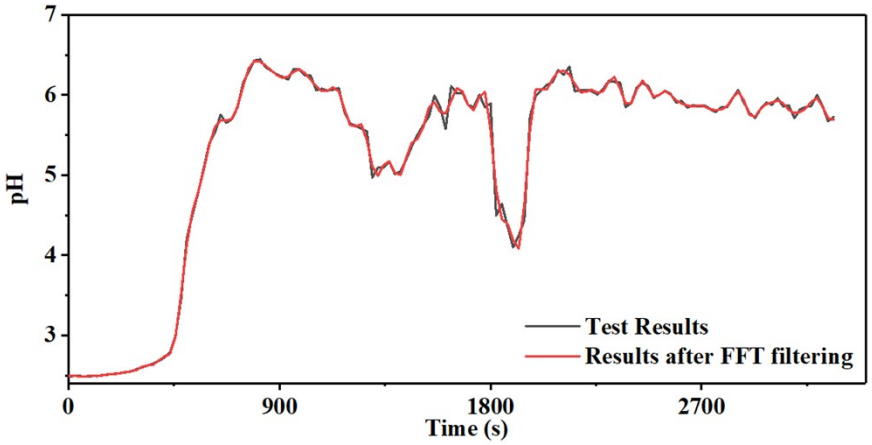

Fig. S13. Test results obtained in reference (V. F. Curto *et al.*, *Sens. Actuators, B* 2012, *175*, 263-270.) during practical exercise and results after FFT filtering.

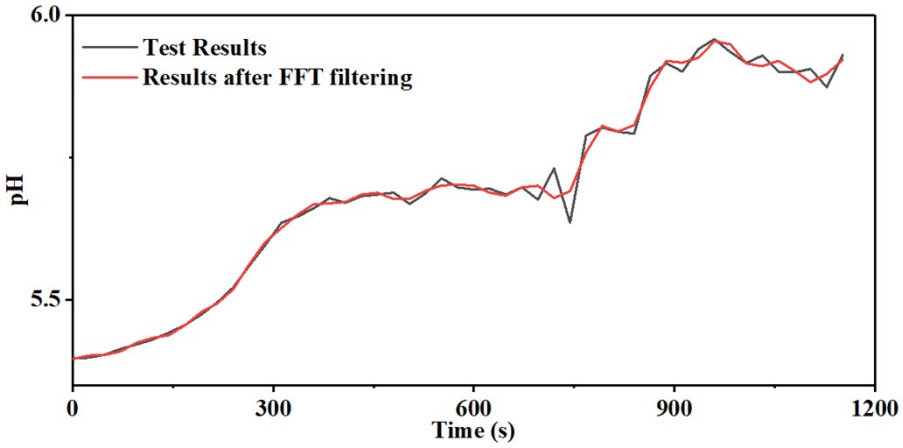

Fig. S14. Test results obtained in reference (G. Wang *et al.*, *IEEE Trans. Biomed. Eng.* 2019, *66*, 1000-1005.) during practical exercise and results after FFT filtering.

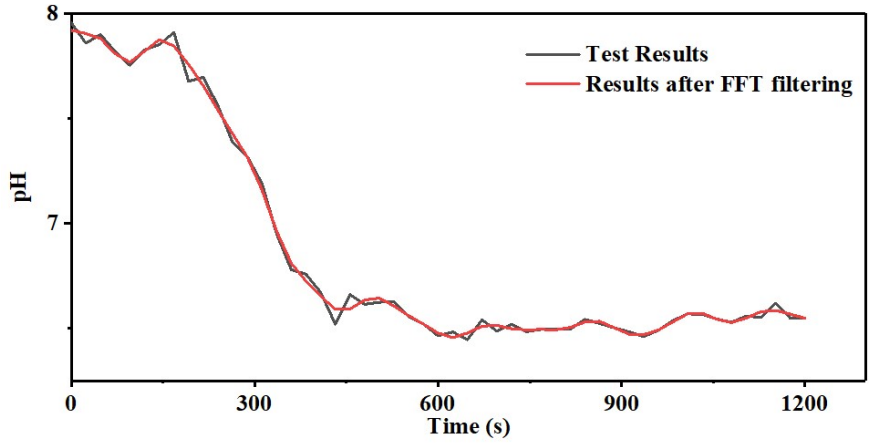

Fig. S15. Test results obtained in reference (P. Escobedo *et al.*, *Sens. Actuators, B* 2021, *327*, 128948.) during practical exercise and results after FFT filtering.

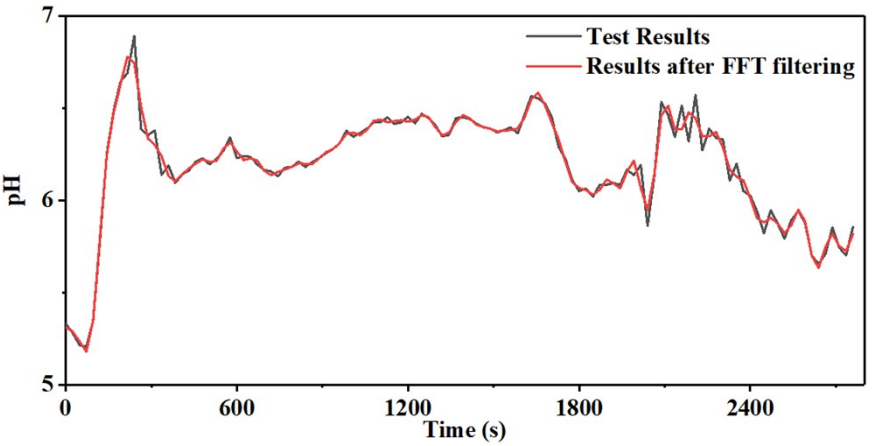

Fig. S16. Test results obtained in reference (S. Anastasova *et al.*, *Biosens. Bioelectron.* 2017, *93*, 139-145.) during practical exercise and results after FFT filtering.

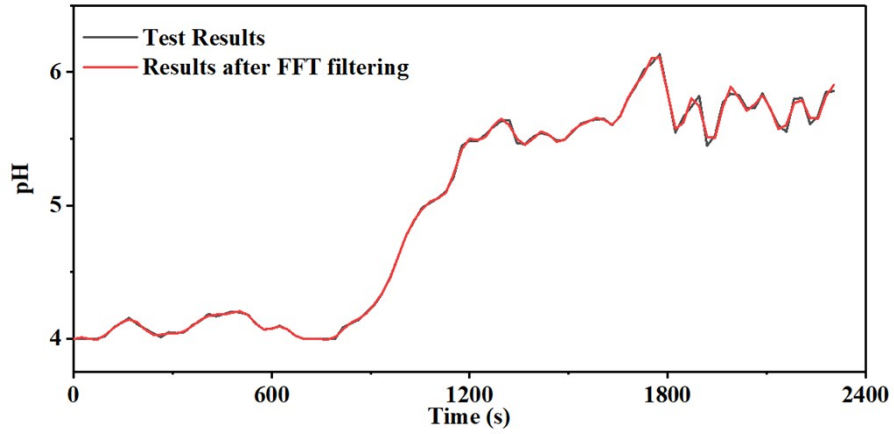

Fig. S17. Test results obtained in reference (D. Morris *et al.*, *Sens. Actuators, B* 2009, *139*, 231-236.) during practical exercise and results after FFT filtering.

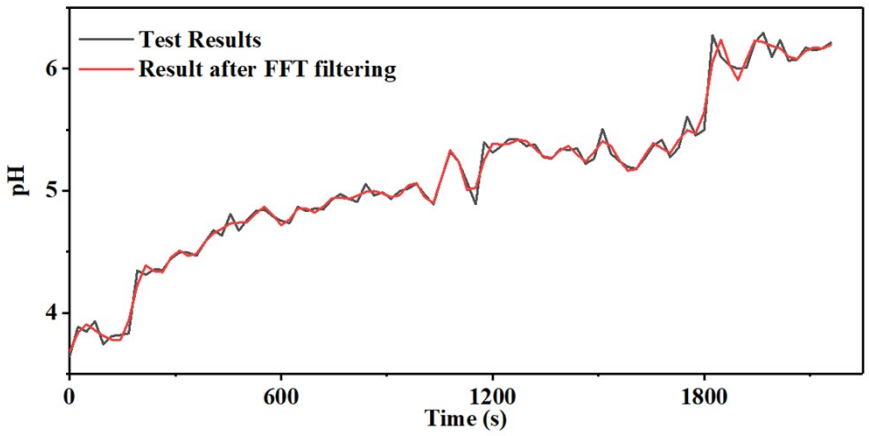

Fig. S18. Test results obtained in reference (M. Caldara *et al.*, *Sens. Actuators, B* 2016, *222*, 213-220.) during practical exercise and results after FFT filtering.

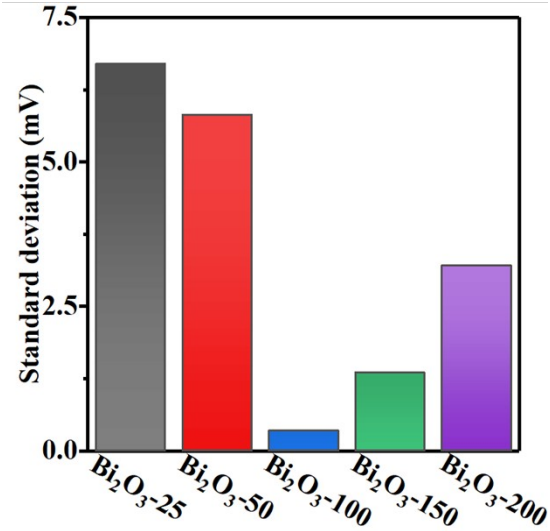

Fig. S19. Standard deciation of $\Delta V_{p\text{-}n}$ during cyclic voltammetry scanning for 20 minutes.

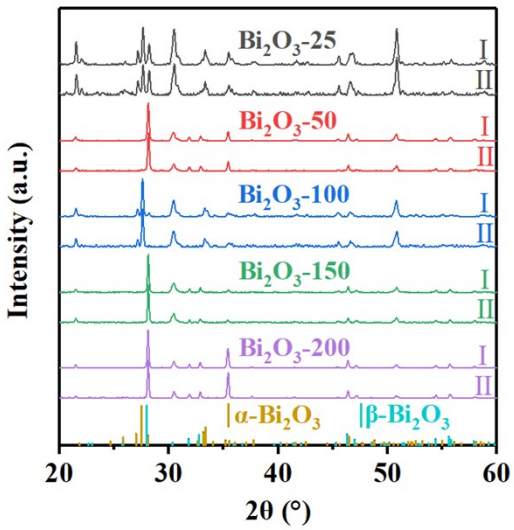

Fig. S20. XRD spectra of Bi_2O_3-25, Bi_2O_3-50, Bi_2O_3-100, Bi_2O_3-150 and Bi_2O_3-200 before (I) and after (II) 20 minutes PEC stability test.

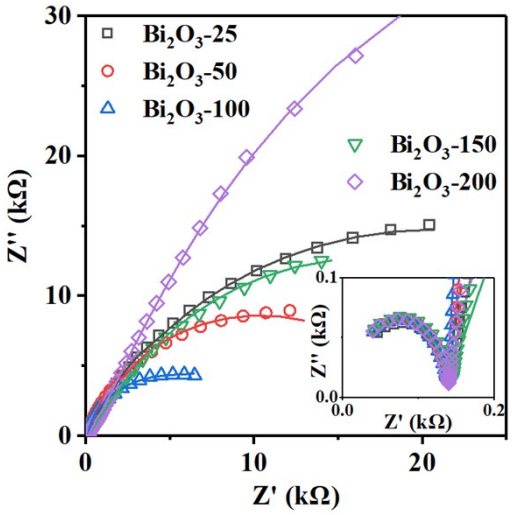

Fig. S21. Nyquist diagram for Bi_2O_3-25, Bi_2O_3-50, Bi_2O_3-100, Bi_2O_3-150 and Bi_2O_3-200 under illumination (415 nm, 35 mW cm^{-2}) at open circuit potential in artificial sweat with pH 6.

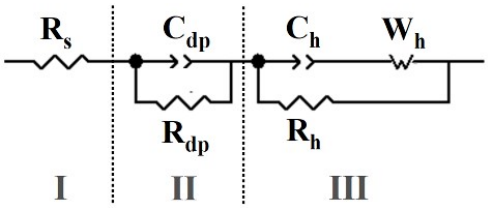

Fig. S22. The equivalent electrical analogs used for modeling the PEC cell; R_S represents the resistance of the transparent conductive substrate and the external contact resistance of the cell (I); C_{dp} and R_{dp} are the chemical capacitance and resistance of depletion layer, respectively (II); R_h describes the charge transfer resistance in the Helmholtz layer; C_h and W_h elements characterize the recharged Helmholtz layer and Warburg diffusion impedance, respectively (III).[3]

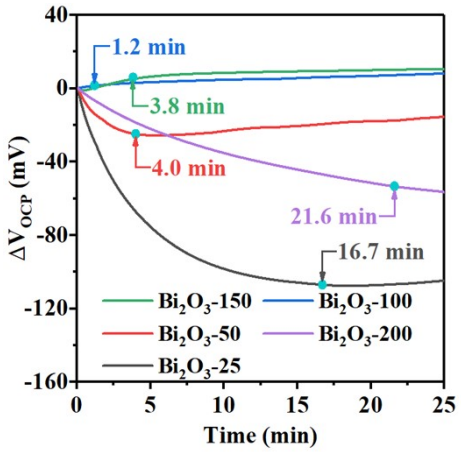

Fig. S23. The change of ΔV_{OCP} under illumination of Bi_2O_3-25, Bi_2O_3-50, Bi_2O_3-100, Bi_2O_3-150 and Bi_2O_3-200 in artificial sweat with H_2O_2.

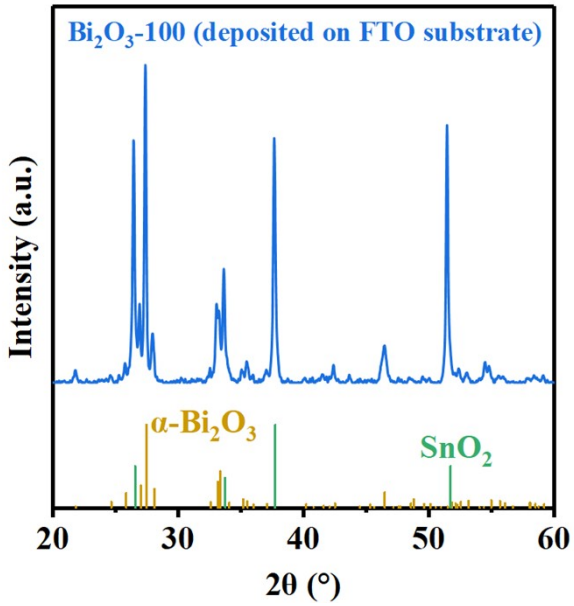

Fig. S24. XRD spectra of Bi_2O_3-100 (deposited on FTO substrate). Except for the peak of FTO substrate (SnO_2), other peaks can correspond to α-Bi_2O_3 (PDF # 76-1730), so this film is a pure α-Bi_2O_3.

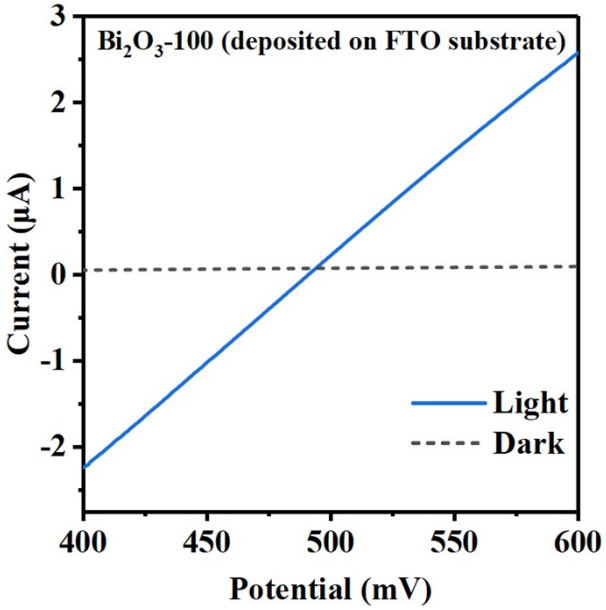

Fig. S25. Cyclic voltammetry scans for Bi_2O_3-100 (deposited on FTO substrate) under light and dark. It was found that it possesses the characteristic of p-type and n-type transition.

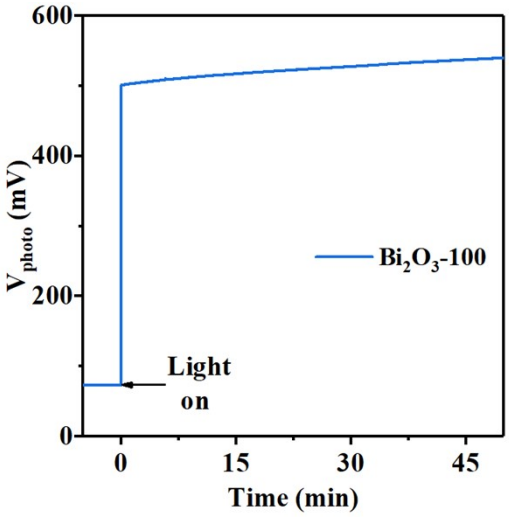

Fig. S26. Open circuit potential of Bi_2O_3-100 under chopped illumination (415 nm, 35 mW cm^{-2}) in artificial sweat with pH 6.

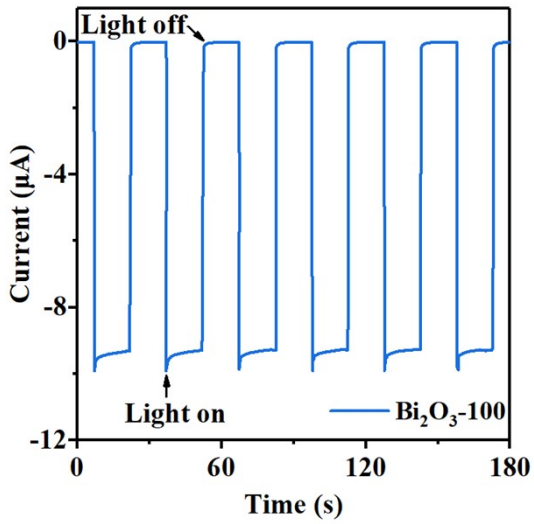

Fig. S27. Unbiased current of Bi_2O_3-100 under chopped illumination (415 nm, 35 mW cm^{-2}) in artificial sweat with pH 6.

Supplementary tables

Table. S1. Comparison of some flexible electrochemical pH sensors.

Material of working electrode	Preparation method of working electrode	Sensitivity (mV pH^{-1})	Anti-interference characteristics	Biocompatibility	Goodness of Fit (R^2)	Application	References
Carbon-uric acid composite	Manual pad printing	72.7	Resist the interference of ascorbic acid	-	0.990	Wound pH	4
Carbon	Pencil-drawn	26.9	Resist the interference of sensor bending	-	0.976	-	5
PdO/Pd/Au/PMMA[a]	Electrospinning, magnetron sputtering, electrochemical deposition and thermal oxidation	18.0	Resist the interference of sensor bending	-	0.921	Sweat pH	6
SiO_X/Al_2O_3/InGaZnO	Spin-coated, sputtering, wet etching, atomic layer deposition and electron beam evaporation	240.0[b]	Resist the interference of sensor bending	-	-	Sweat pH	7
PANi/PEDOT:PSS/ MWCNT[c]	Dipping, drying and electrochemical deposition	61.0	Resist the interference of ions (NH^{4+}, Mg^{2+}, Ca^{2+}, K^+ and Na^+)	Good	-	Sweat pH	8
Graphite-polyuretane/graphene	Spin-coated, electron beam evaporated and wet etching	11.1	Resist the stretching of the electrode and the interference of ions (K^+, Na^+) and glucose.	-	-	Sweat pH	9
IrO_2	Electrochemical deposition	47.5	-	Good	0.993	Sweat pH	10
Graphite composite	Screen printing	4.0	Resist the interference of sensor bending and the interference of ions (K^+, Na^+)	-	0.989	-	11

			glucose and urea.				
Graphene oxide	Coating	26.3	-	-	0.990	-	[12]
PCSC[d]	Electrochemical deposition and dipping	58.3	Self-healing after scratches.	-	0.998	Sweat pH	[13]
Bi_2O_3	Magnetron sputtering and thermal oxidation	44.4	**Resist the change in the coverage of sweat on photoelectrode, the variation in light intensity, and the bend of photoelectrode.**	Good	0.99965	Sweat pH	This work

[a] PMMA: poly(methyl methacrylate). [b] At 100 accumulation cycles. [c] PANi: polyaniline; PEDOT: poly(3,4-ethylenedioxythiophene); PSS: polystyrene sulfonate; MWCNT: multi-walled carbon nanotubes. [d] PCSC: poly(1,4-cyclohexanedimethanol succinate-co-citrate).

Table. S2. Charge accumulation in space charge region of Bi_2O_3-25, Bi_2O_3-50, Bi_2O_3-100, Bi_2O_3-150 and Bi_2O_3-200.

Samples	Charge accumulation in space charge region (s^{-1} cm^{-2})[a]	Charge injection efficiency (%)
Bi_2O_3-25	1.0×10^{11}	5.06
Bi_2O_3-50	0.46×10^{11}	18.25
Bi_2O_3-100	0.14×10^{11}	42.42
Bi_2O_3-150	0.76×10^{11}	19.36
Bi_2O_3-200	1.01×10^{11}	12.25

[a] Charge accumulation in space charge region = Photocurrent × (1 - Charge injection efficiency) / Charge injection efficiency.

Table. S3. Parameters obtained by fitting the EIS of Bi2O3-25, Bi2O3-50, Bi2O3-100, Bi2O3-150 and Bi2O3-200 using the equivalent electrical analogs in Fig. S21.

Samples	R_s (Ω)	R_{dp} (Ω)	C_{dp} (F)	R_h (Ω)	C_h (F)	W_h (Ω)
Bi_2O_3-25	19.3	116.3	1.32×10^{-9}	38439	4.88×10^{-6}	976.6
Bi_2O_3-50	13.2	124.2	1.29×10^{-9}	18474	1.48×10^{-6}	1011.0
Bi_2O_3-100	10.4	126.6	2.04×10^{-9}	8774	8.17×10^{-7}	718.8
Bi_2O_3-150	16.9	115.6	6.42×10^{-10}	28983	1.50×10^{-5}	218.5
Bi_2O_3-200	15.9	115.0	7.33×10^{-10}	62866	9.94×10^{-6}	285.2

References

1 R. C. Dawkins, D. Wen, J. N. Hart and M. Vepsäläinen, *Electrochim. Acta*, 2021, **393**, 139043.
2 R. A. Shafik, M. S. Rahman and A. R. Islam, 2006.
3 T. Lopes, L. Andrade, H. A. Ribeiro and A. Mendes, *Int. J. Hydrogen Energy*, 2010, **35**, 11601-11608.
4 D. Sharp, *Biosens. Bioelectron.*, 2013, **50**, 399-405.
5 R. Kawahara, P. Sahatiya, S. Badhulika and S. Uno, *Jpn. J. Appl. Phys.*, 2018, **57**, 04FM08.
6 V. C. Diculescu, M. Beregoi, A. Evanghelidis, R. F. Negrea, N. G. Apostol and I. Enculescu, *Sci. Rep.*, 2019, **9**, 1-12.
7 S. Nakata, M. Shiomi, Y. Fujita, T. Arie, S. Akita and K. Takei, *Nat. Electron.*, 2018, **1**, 596-603.
8 R. E. Smith, S. Totti, E. Velliou, P. Campagnolo, S. M. Hingley-Wilson, N. I. Ward, J. R. Varcoe and C. Crean, *Sens. Actuators, B*, 2019, **287**, 338-345.
9 W. Dang, L. Manjakkal, W. T. Navaraj, L. Lorenzelli, V. Vinciguerra and R. Dahiya, *Biosens. Bioelectron.*, 2018, **107**, 192-202.
10 M. L. Zamora, J. M. Domínguez, R. M. Trujillo, C. B. Goy, M. A. Sanchez and R. E. Madrid, *Sens. Actuators, B*, 2018, **260**, 601-608.
11 L. Manjakkal, W. Dang, N. Yogeswaran and R. Dahiya, *Biosensors*, 2019, **9**, 14.
12 S. Søpstad, K. Imenes and E. A. Johannessen, *IEEE Sens. J.*, 2019, **20**, 599-609.
13 J. H. Yoon, S.-M. Kim, H. J. Park, Y. K. Kim, D. X. Oh, H.-W. Cho, K. G. Lee, S. Y. Hwang, J. Park and B. G. Choi, *Biosens. Bioelectron.*, 2020, **150**, 111946.